Cyclic capacity of monopiles in sand under partially drained conditions: Numerical approach

Hans Petter Jostad1, Haoyuan Liu2, Nallathamby Sivasithamparam3, and Raffaele Ragni4

1Norwegian Geotechnical Institute, Oslo, Norway.

2Norwegian Geotechnical Institute, Oslo, Norway. Emali: haoyuan.liu@ngi.no

3Norwegian Geotechnical Institute, Oslo, Norway.

4Norwegian Geotechnical Institute Perth, Australia.

ABSTRACT

Cyclic loading of saturated sand under partially drained condition may lead to accumulated strains, pore pressure build-up and consequently reduced effective stresses, stiffnesses and shear strengths. This will affect the ultimate limit state (ULS) capacity of monopile foundations in sand for offshore wind turbines (OWTs). This paper calculates the performance of a large diameter monopile foundations, which is installed in a uniform dense sand, subjected to a storm loading using the Partially Drained Cyclic Accumulation Model (PDCAM). The simultaneous pore pressure accumulation and dissipation is accounted for by fully coupled pore water flow and stress equilibrium (consolidation) finite element analyses. Drainage and cyclic load effects on monopile behaviour are studied by comparing the PDCAM simulation results with simulation results using Hardening Soil model with small strain stiffness (HS-Small). At the end, a simplified procedure of PDCAM – named as PDCAM-S is proposed and the results using this approach together with PLAXIS 3D and the NGI-ADP soil model are compared with the PDCAM results.

INTRODUCTION

In design of monopile foundations for offshore wind turbines (OWTs), the Ultimate Limit State (ULS) condition, i.e., sufficient capacity or tolerable displacements, needs to be checked. Originally, this was done using API (API 2014) soil support springs developed for design of other types of offshore structures as, for instance, jacket platforms used in the oil and gas industry. However, it is well accepted nowadays that the API soil support springs developed for long slender piles are not suitable for large diameter piles with length to diameter ratios (L/D) typically smaller than 5 (DNV 2016). New formulations for soil supports were developed based on large-scale model tests together with finite element analysis (FEA) in, for instance, the PISA project (Byrne et al. 2019). The PISA soil support springs are calibrated based on the push-over analyses results, where the non-linear stress-strain relationship of clay layers is modelled by the stress-path dependent NGI-ADP soil model (Grimstad et al. 2012) and sand layers by the Hardening Soil model with small strain stiffness (HS-Small) (Schanz et al. 1999). There, the clay layers are assumed to be undrained while the sand layers are assumed to be drained.

In many 3D FE analyses on OWT foundation cyclic behaviour, fully drained conditions are assumed (Liu et al. 2021). However, it has been demonstrated by FEA (Li et al. 2019; Erbrich et al. 2010; Jostad et al. 2020) that the behaviour of sand during at least a single load cycle is closer to be undrained. Furthermore, for fine sand and sand with fines content, the behaviour is even close to undrained during several load cycles. This may therefore lead to pore pressure build-up, and consequently reduced effective stresses, stiffnesses and shear strengths. DNV (2016) requires that the effect of cyclic loading should be considered in the design of monopile foundations. The effect of cyclic loading under partially drained conditions may give increased or reduced capacity compared to the drained capacity depending on the sand (relative density D_r, grain size distribution, fines content, etc.) and the actual storm loading history. 'Partially drained' in this paper is used to describe the situation where pore pressure accumulation and dissipation occurs simultaneously – which is different from the fully drained and perfectly undrained conditions.

To account for the effect of cyclic loading in clay and sand layers, NGI has developed two finite element calculation procedures, namely the Undrained Cyclic Accumulation Model (UDCAM) (Jostad et al. 2014) and Partially Drained Cyclic Accumulation Model (PDCAM) (Jostad et al. 2015). UDCAM and PDCAM are based on a methodology developed from the beginning of the 1980s to consider the effect of cyclic loading due to waves on gravity-based structures (GBS) used by the oil and gas industry (Andersen et al. 1988). A key parameter in the two methodologies is the equivalent number of undrained cycles (N_{eq}) of the largest cyclic shear stress that accounts for the effect of the cyclic stress history of the entire storm.

The main purpose of this paper is to demonstrate the effect of cyclic loading on the capacity of a large diameter monopile foundation in a uniform dense sand under partially drained and undrained conditions for the DTU 10-MN reference wind turbine in the North Sea, subjected to a representative peak storm history (Bachynski et al. 2019). The lateral displacement of the monopile foundation (used to check monopile capacity in this work) is calculated by PDCAM. To check the validity of the assumptions in some well accepted design methods – for instance assume fully drained behaviour for sandy soil layer and not fully address the effects of cyclic loading, the PDCAM simulation results are compared with the conventional drained push-over analysis using PLAXIS 3D and the HS-Small model (Brinkgreve et al. 2016; Schanz et al. 1999).

Finally, a simplified calculation procedure that accounts for cyclic loading under partially drained condition, named PDCAM-S, is proposed as a practical monopile design tool.Use of PDCAM and PDCAM-S requires a constitutive model can capture reliably soil undrained stress-strain response at a given number of cycles. Constitutive models such as hypoplasticity model (Niemunis and Herle 1997) and bounding surface model (Liu et al. 2020) can also be used for the purpose. In this work, NGI-ADP model (Grimstad et al. 2012) is selected. The advantage of using NGI-ADP model is that the model can capture the change of the direction of the major principal stress in different soil elements adjacent to the pile shaft (as shown in Grimstad et al. (2012)). Besides, this paper aims to provide a convenient simulation tool for industrial design. NGI-ADP model is available in the widely used FE software PLAXIS 3D. However, the validation of PDCAM and PDCAM-S procedures (as well as 3D FE analysis using both implicit and explicit constitutive models) suffer from the lack of suitable model tests with combined pore pressure accumulation and dissipation representative for the soil around monopiles. PDCAM and PDCAM-S procedures are considered as reasonable based on the facts that: (1) the undrained stress-strain and pore pressure responses of the soil at different cyclic and average shear stresses and number of cycles are directly from the lab test data and their interpolation; (2) the dissipation of the generated pore water pressure is taken in account through the well-accepted consolidation theory.

BRIEF DESCRIPTION OF PDCAM

The PDCAM model described in Jostad et al. (2015) may be used to calculate strain accumulation, pore pressure build-up, reduction in cyclic shear modulus and shear strength of a sand subjected to an idealised load history. The pore pressure accumulation procedure (Andersen 2015) is used to calculate the number of undrained cycles, N_{eq}, of a cyclic shear stress τ_{cy} that generates an accumulated pore pressure u_{acc}, as illustrated in Fig. 1 and being explained in Stewart (1986) (for the accumulation strains).

The key assumption of the principle of equivalent number of cycles can be described as follows: for a given normalised average shear stress τ_a/p'_0 (where p'_0 is the initial mean effective stress prior to cyclic loading), all combinations of normalised cyclic shear stress τ_{cy}/p'_0 and number of cycles N (i.e., τ_{cy}/p'_0 and N pair) that give the same normalised accumulated pore pressure u_{acc}/p'_0, are assumed to be at the same state. This assumption is used to transfer an idealised composition of parcels of different constant τ_{cy}/p'_0 to an equivalent number of cycles (N_{eq}) of the normalised largest cyclic shear stress (as illustrated in Fig. 1).

At this equivalent stress state, the average (γ_a), accumulated (γ_{acc}) and cyclic (γ_{cy}) shear strain are assumed to be the same as the corresponding strain components after the entire shear stress history was applied (i.e., $\gamma_a = \gamma_{a,eq}$, $\gamma_{acc} = \gamma_{acc,eq}$ and $\gamma_{cy} = \gamma_{cy,eq}$). The cyclic shear stress

τ_{cy} is defined as $\tau_{cy} = (\tau_{peak} - \tau_{trough})/2$, where the subscripts 'peak' and 'trough' represent the peak value and the trough value of the corresponding variables. Similarly, the cyclic shear strain $\gamma_{cy} = (\gamma_{peak} - \gamma_{trough})/2$; the average shear stress $\tau_a = (\tau_{peak} + \tau_{trough})/2$ and the average shear strain $\gamma_a = (\gamma_{peak} + \gamma_{trough})/2$ are defined. The accumulated shear strain (γ_{acc}) is the increase in average shear strain due to cyclic loading. In triaxial condition, shear stress $\tau = (\sigma'_a - \sigma'_r)/2$; shear strain $\gamma = \varepsilon_a - \varepsilon_r$, where σ'_a, σ'_r, ε_a and ε_r denote the axial effective stress, radial effective stress, axial strain and radial strain, respectively.

The accumulated pore pressure, average and cyclic shear strains as function of number of undrained cycles of constant normalised cyclic shear stress under a given normalised average shear stress are presented in contour diagrams (Andersen 2015) that are established from a set of cyclic tests consolidated to different average shear stresses τ_a and mean effective stress p'_0, and then subjected to a cyclic shear stress τ_{cy} under undrained condition. An example of a contour diagram cross-section is shown in Fig. 2a, namely, normalised accumulated pore pressure, u_{acc}/p'_0, as a function of number of cycles and normalised cyclic shear stress, τ_{cy}/p'_0. A similar diagram of contours of cyclic shear strain is shown in Fig. 2b. These diagrams are based on results from triaxial tests on clean Dogger Bank sand with a relative density $D_r = 80\%$ presented in Blaker and Andersen (2019), where a ratio $\tau_a/p'_0 = 0.43$ was used.

The simultaneous reduction in the accumulated pore water pressure u_{acc} due to pore pressure dissipation is accounted for by a fully coupled stress equilibrium and pore water flow (consolidation) formulation (Jostad et al. 2015). The analyses are run in time domain, with time increments corresponding to a specified number of cycles of constant global cyclic load. The normalised cyclic shear stress (τ_{cy}/p'_0) in all integration points around the monopile under the global loads is calculated in an independent FEA. The u_{acc} under undrained condition in each integration point is found from the pore pressure contour diagram based on the updated number of cycles (current equivalent number of cycles, $N_{eq,i}$ plus the additional number of cycles N_{i+1} due to the change of τ_{cy}/p'_0 in the time increment) as shown in Fig. 1.

The pore pressure increment Δu_{acc} is transferred to a volumetric strain increment $\Delta\varepsilon_{vol,acc}$

by dividing it by a mean-effective-stress-dependent reloading bulk modulus K_r, i.e., $\Delta\varepsilon_{vol,acc} = \Delta u_{acc}/K_r$. The mean effective stress change $\Delta p'$ for the actual time increment is than calculated as:

$$\Delta p' = K_r(\Delta\varepsilon_{vol} - \Delta u_{acc}/K_r) \tag{1}$$

The resulting mean effective stress reduction $\Delta p'$ and volumetric strain increase $\Delta\varepsilon_{vol}$ are automatically found by the coupled consolidation formulation. It is seen from the above equation that $\Delta p' = -\Delta u_{acc}$ for perfectly undrained condition ($\Delta\varepsilon_{vol} = 0$) and $\Delta\varepsilon_{vol} = \Delta u_{acc}/K_r$ for fully drained condition ($\Delta p' = 0$).

For non-linear consolidation problems (e.g. $K_r \sim k \sim$ nonlinear average shear stress-strain relationship, where k is the void-ratio-dependent permeability), a global iteration scheme is used to satisfy stress equilibrium and ensure consistency in the amount of pore water flow within the time increment (Potts et al. 2001). The increase in pore pressure accounting for pore pressure dissipation (Δu) and volumetric strain increase ($\Delta\varepsilon_{vol}$) can be calculated as:

$$\Delta u = \frac{\Delta u_{acc}}{1 + \dfrac{M_r k \Delta t}{\gamma_w L_d H_{soil}}} \tag{2}$$

$$\Delta\varepsilon_{vol} = \frac{\Delta H_{soil}}{H_{soil}} = \frac{\Delta u_{acc} - \Delta u}{M_r} \tag{3}$$

where L_d is the one-way drainage distance, Δt is the time increment, H_{soil} is the soil sample height. In this calculation, it is assumed that the amount of pore water flow is given by the pore pressure gradient at the end of the time increment (i.e., an implicit formulation). Detailed discussion to the equation can be found in Jostad et al. (2021).

Knowing N_{eq} at a given integration point, the cyclic and average stress-strain relationships are also established from contour diagrams. The shear stress-strain relationships defined by the triaxial contour diagram are transferred to a general 3D stress state by assuming same orientations (coaxiality) between principal total strains and principal effective stresses.

Due to the coupling between average and cyclic shear stresses and strains for a given N_{eq} when calculating the shear strains, the analysis of an idealised storm history in PDCAM is carried out by altering between average and cyclic calculation phases for each load parcel. An average phase is a consolidation analysis starting from the previous cyclic phase. A cyclic phase is an undrained analysis starting from the last average stress state. In this process, N_{eq}, p'_0 and τ_a/p'_0 within each integration point are transferred from an average phase to a cyclic phase, while τ_{cy}/p'_0 in each integration point is transferred from a cyclic phase to an average phase. The detailed description about this coupled calculation procedure can be found in Jostad et al. (2015). This procedure makes it possible to calculate the total (sum of average plus cyclic) displacements of the monopile at the maximum loads, accounting for the effect of pore pressure build-up and accumulation of strains due to the storm loading prior to the maximum loads.

PDCAM ANALYSIS

Storm loading

A one-hour peak history (including the maximum loads) during a 35-hour storm load sequence at a water depth of 30 m in the North Sea (Bachynski et al. 2019) is considered. The significant wave height, peak wave period and wind speed at the location are based on hind-cast data. The calculated time history of bending moment and horizontal force at seabed are for the DTU 10-MW reference wind turbine with a hub height of $119m$ above seabed during idling (shut down). The wave and wind directions are assumed to be aligned. The loads are calculated for a monopile with a diameter of $9m$ that extends 36 m beneath seabed. Any effects of cyclic degradation of the soil are neglected in the calculations of the loads. Thus, the coupling between seabed loads and foundation stiffness is neglected in the analyses.

From the one-hour peak storm history, an idealised load composition containing 12 load parcels with increasing constant cyclic load amplitude is established by the Rainflow counting method (Matsuishi and Endo 1968). The maximum resultant cyclic horizontal force is $13.8MN$, acting 27 m above seabed and the resulting cyclic bending moment at seabed is $372MNm$. The number of load cycles (N) at different load levels (expressed as a fraction of the maximum cyclic load) within the different parcels is presented in Table 1. The average loads in this load history are small and, therefore, for simplicity taken equal to zero. The dominating cyclic load frequency of the history is about $0.25Hz$ (i.e., cyclic loading period of $T_p = 4s$). Thus, the duration of the idealised load composition is 1.3 hour instead of one-hour.

Material properties

Test results from drained monotonic and cyclic undrained triaxial tests on a clean Dogger Bank sand with a relative density of 80% were used to establish contour diagrams of cyclic and average shear strains and normalised accumulated pore pressure as a function of number of undrained cycles of different normalised cyclic shear stress (Blaker and Andersen 2019). Examples of representative triaxial cross-sections at an average normalised shear stress $\tau_0/p'_0 = 0.43$, based on a horizontal earth pressure coefficient of $K_0 = 0.45$, are shown in Figs 2a and 2b. These contour diagrams are digitised (points of τ_a/p'_0, τ_{cy}/p'_0, γ_{cy}, γ_a, u_{acc}/p'_0 and N) and used as input in PDCAM. From these figures one may extract non-linear normalised shear stress-strain curves for different cycles as shown in Fig. 3 and normalised accumulated pore pressure curves versus number of cycles for different normalised cyclic shear stresses. However, PDCAM interpolates directly between the digitised points.

A representative reloading bulk modulus $K_r = 100MPa$ is established from the oedometer tests on the sand using the interpretation presented in Jostad et al. (2020). To transfer the odometer modulus to the bulk modulus, a Poisson ratio $\nu = K_0/(1 + K_0) = 0.31$ is used (i.e., $K_0 = 0.45$). An isotropic coefficient of permeability, $k = 5 \times 10^{-6} m/s$, is taken from Blaker and Andersen (2019).

To ease comparison of the results obtained, for instance, against the dissipation data presented in Li et al. (2019) is used – that is, a coefficient of consolidation $c_v = 0.079m^2/s$ is adopted in PDCAM-S simulation as presented in the following part of this paper. For PDCAM simulation, same c_v value is achieved by using a constant oedometer modulus of $M_r = 158MPa$. However, PDCAM can use a general mean effective stress dependent bulk modulus that varies from virgin loading, to unloading and reloading (Jostad et al. 2020).

Finite element model

NGI's in-house FE program, Bifurc3D, is used in the analyses in order to streamline the PDCAM calculation process, i.e., the coupling between the average and cyclic calculation phases for the different load parcels and manual control of the time increments within the different load parcels.

The finite element model is generated by the pre-processor Femgv (Femsys Limited 1999). An example of a finite element mesh is shown in Fig. 4. Due to the symmetry, only half of the boundary value problem is modelled. The distance to the outer boundaries from the vertical centre line is $45m$ (5 times the pile diameter D). The presented mesh contains 1072 20-noded iso-parametric brick elements with reduced (2x2x2) Gaussian integration. The soil elements have excess pore pressure degrees of freedom in the 8 corner nodes, besides the 3 displacement degrees of freedom in all nodes. The nodes at all vertical boundaries are fixed in the direction normal to the boundary surface, and at the bottom boundary in all directions. Free drainage (i.e., zero excess pore pressure) is prescribed at the top and vertical outer boundaries. The horizontal load (half of the total load) is applied to the monopile at $27m$ above seabed.

The monopile has the following properties: outer diameter $D = 9m$, constant wall thickness of $0.1m$ and Young's modulus $E = 210GPa$. In Bifurc 3D, the monopile is modelled as a solid pile. To maintain the same bending stiffness (i.e., $EI = 5538GNm^2$) as the actual tubular pile, the solid pile has an equivalent Young's modulus $E^* = 17.2GPa$ and Poisson's ratio 0.3. The contribution of the stiffness and drainage of the soil within the monopile is for simplicity neglected. Pile head displacements calculated using solid pile and tubular pile are compared – a difference of about 10% is expected under the same ULS load level. Such a difference is not important under the premise of qualitative comparisons.

Both physical modelling results (Fan et al. 2021) and numerical simulation results (Staubach et al. 2021) reveal that pile installation affects pile stiffness and bearing capacity to an extent. In the current work, the soil-steel interface is for simplicity simulated as a rough interface since the effect of installation may increase or decrease the actual interface strength depending on the installation method together with the sand properties. To include any effects from the installation, the actual installation process needs to be considered and its effect to be accounted for in the analysis. Due to the rapid two-way cyclic loading, no tensile gaps are assumed along the monopile. However, in an actual design situation, the validity of this assumption, together with the limitation due to cavitation cut-off in the pore water need to be considered (Jostad et al. 2020).

Results

Reference cases with constant N_{eq}

As references, the cyclic lateral displacements of the monopile with embedded length $L = 15m$ ($L/D = 1.667$) and $L = 18m$ ($L/D = 2$) are first calculated with different assumed uniform $N_{eq} =$ 1, 10 and 25 (simulation case N_{eq}=25 only applies to the pile with $L/D = 2$) of the maximum cyclic storm load within the entire soil volume. Thus, only the cyclic phase with the load in parcel 12 (see Table 1) is analysed with input of the initial effective mean stress, $p_0 = \frac{1+2K_0}{3}\gamma' z = 6.33z\ kN/m^2$, $\tau_a/p'_0 = 0.43$ and the considered N_{eq} in each integration point.

The cyclic shear strain γ_{cy} versus normalised cyclic shear stress τ_{cy}/p'_0 for $N = 1$, 10 and 100 are provided in Fig. 3, for undrained cyclic triaxial test. The curves are extracted from the contour diagram in the cross section shown in Fig. 2b. It should be noted that the upper part of the curves (above $\tau_{cy}/p'_0 = 1.2$) at low N (< 10) is uncertain, since the curves are extrapolated beyond the tested cyclic shear stress range from the laboratory tests. Therefore, also the results from the undrained monotonic triaxial compression and extension tests shown in Jostad et al. (2020) are included. Based on these results, it is believed that the extrapolations give cyclic shear strengths on the low side at low N-values.

Fig. 5 shows the calculated cyclic lateral displacement at seabed versus the cyclic horizontal load. In the figure, a vertical line corresponding to $0.1D = 0.9m$ is also shown. The cyclic lateral displacement is increasing from about $0.12m$ to $1.24m$ when N_{eq} is increasing from 1 to 10 for $L = 15m$ ($L/D = 1.667$, Fig. 5a). For $L = 18m$ ($L/D = 2$), the cyclic lateral displacement increased from $0.07m$ to $1.03m$ from $N_{eq} = 1$ to $N_{eq} = 25$ (Fig. 5b). This demonstrates the importance of evaluating the effect of cyclic loading (e.g. equivalent number of undrained cycles) on the capacity (or displacement) of large diameter monopiles in sand.

One-hour peak storm load history

PDCAM analyses of the one-hour peak storm are performed for three different embedded monopile lengths over diameter ratios L/D = 1.667, 2 and 2.22. Each load parcel is analysed by an average and a cyclic phase as described before. As reference, the response assuming perfectly undrained conditions is also analysed for the different monopile embedded lengths. The calculated cyclic lateral monopile displacement at seabed under the maximum load at the end of the load history for the different L/D-ratios and drainage conditions are shown in Fig. 6. To satisfy a displacement criteria of less than $0.1D$, the required embedded length is about $L/D = 1.75$. For undrained conditions, this length had to be increased to about $L/D = 2.15$ (based on linear interpolation between the two data points available).

The calculated cyclic lateral displacement of $0.29m$ for $L/D = 2$ corresponds roughly to a constant uniform equivalent number of undrained cycles of $N_{eq} = 9$ based on logarithmic interpolation in N between the curves in Fig. 5b. This value ($N_{eq} = 9$) could be compared with the calculated distribution of the equivalent number of cycles before application of the maximum load shown in Fig. 7. It is seen that $N < 10$ in a large volume around the monopile. The equivalent number of cycles for the undrained case is much larger at the end of the load storm – which is in line with larger pore water pressure.

The corresponding accumulated pore pressure distributions are shown in Fig. 8. The undrained and partially drained simulations give similar pore water pressure distribution pattern. Only, the pore pressure under partially drained condition is slightly smaller than the pore pressure accumulated under undrained condition.In the plot, the color change 'inside' the monopile is due to the plotting issue of the software – no pore water pressure should be accumulated inside the equivalent solid pile in this work.

The reduction in effective mean stresses p' around the monopile is therefore also rather similar for the partially drained and undrained case as shown in Fig. 9 at four depths (z/D = 0.375, 0.625, 0.875 and 1.13) at integration points close to the centerline in the front of (i.e., along the primary loading direction) the monopile.

The normalised accumulated pore pressure at the end of the storm (loci of end points) for these four points, both partially drained and undrained, are included in the pore pressure contour diagram in Fig. 10. Based on these points, the equivalent number of cycles (N_{eq}) is varying between 9 and 30 for the partially drained condition and between 30 and 50 for the undrained condition.

ANALYSES USING THE HS-SMALL MODEL

The PISA project (Byrne et al. 2019) aimed to propose monopile design method for relative small L/D (under 6) ratio. To calibrate PISA soil springs, PLAXIS has developed a numerical tool - MoDeTo (Monopile Design Tool) (Brinkgreve et al. 2020). In PISA method, the sand layer is assumed to be drained. Hardening Soil Small Strain model (i.e., HS-Small model proposed by Schanz et al. (1999)) is suggested to be the simulating consitutive model for the purpose.

To study the possible effects of cyclic loading and pore water pressure, the above lateral monopile displacements obtained using PDCAM is compared with a 'PISA' type analysis for sand. In detail, drained push-over analyses of the same pile are performed using PLAXIS3D and HS-Small model. The same DoggerBank sand are used. The maximum cyclic load within the entire load history is applied $27m$ above seabed but neglecting any excess pore pressure response during application of the maximum cyclic loads, even for the case with a period for the storm history considered here of only 4 seconds. These analyses also neglects any changes in void ratio or redistribution of average effective stresses due to the cyclic loads prior to the peak storm loads.

The material properties of the model are calibrated based on drained monotonic triaxial compression and extension tests presented in Blaker and Andersen (2019), together with the oedometer test as reported by Jostad et al. (2020). The parameter set used in the analyses are shown in Table 2. The finite element model for $L/D = 2$ is shown in Fig. 11. The model consists of 18049 10-noded tetrahedral elements. In this case, only half of the problem is modelled due to geometry symmetry.

The calculated lateral displacements at seabed of monopiles with L/D of 1.5, 1.67, 2.0, 2.22 and 2.5 versus the horizontal load applied $27m$ above seabed are shown in Fig. 12a, whereas Fig. 12b shows the peak load assumed at the maximum lateral displacement allowed of $0.1D = 0.9m$, versus the normalised monopile length. Based on linear extrapolation of these results, the required monopile length is only $12.5m$ ($L/D = 1.39$, as indicated by the red star in Fig. 12b). This is shorter than compared to the results obtained by PDCAM (which required $L/D \approx 1.75$), since build-up of excess pore pressure due to cyclic loading is entirely neglected.

The comparison between PDCAM simulation results and HS-Small results suggests that neglecting the cyclic load and pore water pressure effects may lead non-conservative design of monopile in terms of ULS check.

SIMPLIFIED PDCAM PROCEDURE (PDCAM-S)

The PDCAM method can practically consider the cyclic load effects and gives detailed pore water pressure distribution in the soil domain. However the PDCAM program so far is only serving as a NGI in-house program and has relatively high computational cost. To easily consider partial drainage consideration in monopile industrial design, a more practical and light tool is developed based on the same theoretical framework – i.e., the simplified PDCAM procedure PDCAM-S.

Procedure

In this proposed simplified procedure, the soil domain is divided into multiple sub-layers. PDCAM-S is a simplification of the PDCAM approach, where N_{eq} is calculated at each integration point. This simplification results in a significant reduction of computational time. The load composition, here taken as a number of cycles of different cyclic lateral soil reaction for each sub-layer is derived from non-linear 3D finite element analyses. The cyclic non-linear shear stress-strain relationship within each sub-layer is fitted to the data in the cyclic shear strain contour diagram for an equivalent number of cycles. Due to the coupling between the cyclic soil reactions used to calculate N_{eq} and the cyclic shear stress-strain relationship, these analyses need to be repeated until the solution converges to an accepted accuracy. The pore pressure accumulation for undrained condition is determined from a representative pore pressure contour diagram as, for instance, shown in Fig. 2a.

The simultaneous pore pressure dissipation within each sub-layer is accounted for using curves of degree of drainage, for instance established from finite element analyses. Fig. 13 shows an example of the degree of drainage within a horizontal disc with the cross-section of the impermeable monopile in the middle, as function of the normalised time, $T = t\frac{c_v}{D^2}$, where t is the time of dissipation, $c_v = kM_r/\gamma_w$ is the consolidation coefficient for reloading. This curve was established based on finite element analyses presented in Li et al. (2019). However, more site-specific dissipation curves accounting for soil layering and drainage toward seabed (i.e., combining vertical and horizontal pore water flow) may be established using a full 3D finite element model of the monopile and the surrounding soil. The pore pressure accumulation, i.e. calculation of equivalent number of undrained cycles for the established load composition, may be performed manually or using the method described in Andersen (2015).

The cyclic lateral soil reaction composition for each sub-layer is extracted from the FEA by applying the cyclic loads in increments of the peak values according to the load levels in the actual load composition (Table 1). The resultant lateral soil reaction forces are extracted as the difference in shear force in the monopile at the top and bottom of each sub-layer at each load level.

At the end of the analysis, the seabed loads may be increased until the maximum cyclic lateral capacity H_{ult} of almost all sub-layers are mobilised. The calculated lateral reaction forces may then be normalised by H_{ult} for each sub-layer. Alternatively, the reaction forces for each sub-layer are normalised by the maximum value (like the global load composition in Table 1). These load compositions are used to calculate the equivalent number of undrained cycles within each sub-layer. This process is repeated until the solution converges to an accepted accuracy.

In detail, the PDCAM-S procedure can be described as following:

1. Rearrange the irregular storm load into regular load history as presented in Table 1 (the global load), get N_{eq} values for each layer using global load;
2. Extract from contour diagram the stress-strain response at a representative cyclic over average stress ratio (one can usually assume the cyclic over average stress ratio equals to the largest cyclic load in the load history) at the determined N_{eq}.
3. Calibrate the constitutive model (in this paper, NGI-ADP model in PLAXIS 3D is adopted) against the extracted stress-strain curve and the calculated cyclic strength.
4. Perform finite element analysis. Apply each load parcel from the load history in a calculation

phase for extracting reaction forces P_{cy} in each layer.

5. The calculated reaction forces for a given layer are normalized by the maximum cyclic lateral load H_{ult} of that layer and construct a local load history/parcel by arranging them in ascending order.
6. The local load history/parcels are used to obtain an updated N_{eq} value. The N_{eq} value is determined at the representative mobilization which is defined by P_{cy}/H_{ult}. This procedure should be done for each layer.
7. Repeat procedures from Step 2 to Step 6 until pile deflection and N_{eq} for each layer converges.

PDCAM-S analyses

The proposed simplified Partially Drained Cyclic Accumulation procedure (PDCAM-S) is used to calculate the cyclic lateral displacement of the monopile for the same load condition and soil condition as used in PDCAM. The analyses are carried out using PLAXIS 3D where the cyclic undrained shear stress-strain curves for the different equivalent number of cycles N_{eq} are fitted with the $NGI-ADP$ model (Grimstad et al. 2012). The shape of the stress-strain curves is given by a mathematical equation, where (i) the normalised initial shear modulus G_0/s_u, (ii) the undrained shear strength s_u and (iii) the shear strain at failure, γ_f, are used to fit the actual curves. Fig. 14 shows the fitted curves for $N = 1$, 3, 10 and 30. Since it was difficult to obtain a good fit of the entire curves, the part with relatively small strain level ($\gamma < 5\%$) of the actual curves was given the largest weight, based on previous experience on monopile analysis. For more accurate analyses, it is therefore recommended that a more suitable material model be adopted, which can give a better fit to the entire curve. The values used to fit the curves are presented in Table 3 and the corresponding NGI-ADP parameters where the curves are normalised by the cyclic undrained shear strength for the actual N_{eq} in Table 4. Isotropic conditions were adopted in the analyses, i.e., identical cyclic shear stress-strain curves from triaxial compression, triaxial extension and DSS stress paths.

Pore pressure accumulation

The analysis for any monopile length starts by first calculating the equivalent number of cycles based on the global load composition in Table 1. It is then assumed that the same shear stress mobilisation is achieved in all sub-layers at a given global load. In addition, it is assumed that all soil elements reach the failure contour (here taken at $\gamma_{cy} = 10\%$) at the peak loads. The inconsistency in these assumptions will be updated later by the iterative procedure described in the previous section. The normalised accumulated pore pressure u_{acc}/p'_0 as function of the normalised cyclic shear stress τ_{cy}/p'_0 and number of cycles N under undrained condition is given by the pore pressure contour diagram in Fig. 2a. The simultaneous reduction in pore pressure due to pore pressure dissipation is found from the curve in Fig. 13. Then u_{acc}/p'_0 is calculated by stepping forwards in time with a time increment, for instance, equal to either a period of ten cycles ($\Delta t = 40s$) if $N > 10$ within the parcel, or equals to the real time period of the parcel ($\Delta t = 4s$) if $N < 10$ within the parcel.

Fig. 15 shows the calculated normalised pore pressure u_{acc}/p'_0 as function of time for four different normalised cyclic shear stresses ($\tau_{cy}/p'_0 = 0.68, 0.85, 1.022, 1.193$) at the peak load. The results at the end of the load history for these four calculations are plotted as a loci of end points in Fig. 16. The corresponding equivalent number of undrained cycles (N_{eq} = 4, 3, 4.1 and 4) is then found by moving vertically down to the x-axis (N). Different values of normalised cyclic shear stress at the peak load are selected until the loci of end points reach the failure line (here taken at $\gamma_{cy} = 10\%$).

To demonstrate the effect of drainage, the analyses are repeated assuming partially drained condition. The development of normalised pore pressures under this condition is shown as dotted lines in Fig. 15, and the corresponding loci of end points in Fig. 16. For undrained conditions, the obtained values are consistently higher than the partially drained cases.

The NGI-ADP model parameters for the obtained N values under partially drained condition are then selected based on logarithmic interpolation of the parameters adopted for $N = 1, 3, 10$ and 30. Once the stress-strain curves of all sub-layers have been calibrated, the peak storm loads are applied to the finite element model.

The adjusted equivalent number of cycles for each sub-layer is then calculated in a similar way as done using the global load composition. The results from these pore pressure accumulation calculations are presented in Table 5. It is seen that after the first iteration, N_{eq} increases from the originally calculated value in the layers near the sea bed and below the pile base (sub-layer 1, 2 and 7) whereas it reduces slightly around the rotation point (sub-layer 4, 5, 6). The almost identical results after iteration 1 and 2 are indicative of convergence of the procedure.

The calculated shear force distribution along the monopile for the load levels given in Table 1 are shown in Fig. 17. These distributions are used to calculate the lateral soil reaction forces in each sublayer. The composition of lateral soil reaction force normalised by the value at the maximum load (i.e., when H_{max} is applied) for each sublayer (i.e., R_P) is presented in Table 6. It is seen that the mobilised R_P value in general increases with increasing global load ratio. On the other hand, the shallower soil layers have larger R_P values than that of deeper layers. The number of cycles at high shear mobilisation (large R_P value) is increasing toward seabed which is the reason for the increased N_{eq} in the upper soil layers (as indicated in Fig. 7). By comparing these compositions with the global load composition, it is seen that the mobilised R_p value in general increases with increasing global load ratio. On the other hand, the shallower soil layers have larger R_p values than that of deeper layers. The number of cycles at high shear mobilisation (large R_p value) is increasing toward seabed which is the reason for the increased N_{eq} in the upper soil layers (as indicated in Fig. 7).

After 2 repetitions (iterations) the cyclic lateral displacement at seabed has stabilised at a lateral displacement of 0.24 m. This result is somewhat smaller than the displacement of 0.31 m obtained by PDCAM, but closer to PDCAM than compared to HS-small that only gave a lateral displacement of 0.06m. The main reason why PDCAM-S gave smaller displacement than PDCAM is expected to be due to the difficulties of fitting the stress-strain curves by the NGI-ADP model, as shown in Fig. 14. In design, one should therefore use input data to PDCAM-S that gives conservative results.

The main advantage of PDCAM-S is that the calculations are more robust and computationally significantly faster than using PDCAM, albeit sacrificing some accuracy in the results. In addition, it may be used together with any suitable finite element programs.

DISCUSSIONS

The Partially Drained Cyclic Accumulation Model (PDCAM) or similar explicit calculation models may be used to account for the effect of cyclic loading on the capacity of monopiles in sand during storm loading. As shown, the effects of cyclic loading are pore pressure build-up, reduction in effective mean stress, cyclic stiffness and capacity – at material level (Liu et al. 2022) and/or foundation level. In addition, for other load conditions, including average load components, it will be accumulation of lateral displacements. PDCAM accounts for these effects based on the local cyclic shear stress levels, average shear stress levels, effective mean stress, degree of drainage and the cyclic load composition.

However, PDCAM does not take into account any changes in fabric (i.e. change in void ratio, reorientation of grains, etc.) that may change the behaviour of the sand compared to the response obtained during the undrained cyclic laboratory tests. For instance, the effect of drainage (small volumetric strains) may affect the rate of pore pressure accumulation, as shown in Jostad et al. (2020), While neglecting the fact that the soil is close to undrained conditions during application of the maximum load within a storm, as generally considered in model tests and assumed in existing soil-spring expressions as API and PISA, may lead to a significant underestimation of the monotonic push-over capacity in dense sand, as shown in Jostad et al. (2020). While neglecting the effect of cyclic loading and pore pressure build-up may overestimate the capacity as shown in this work and in Liu and Kaynia (2021). It is therefore important to estimate the effect of partial drainage and pore pressure build-up due to cyclic loading, whether this is achieved with a more advanced model (see PDCAM) or a more computationally efficient one (see PDCAM-S).

CONCLUSIONS

Monopile response under cyclic loading in saturated sand under partially drained condition may be largely affected by the accumulated strain, pore pressure build-up and consequently reduced effective stresses, stiffnesses and shear strengths within the soil. In addition, the response during a single load cycle may be close to undrained, which for dense sands may result in a significant increase in the shear strength due to shear-induced negative excess pore pressure (dilatancy). Therefore, the capacity of a monopile in sand or a soil profile dominated by sand may be higher or lower than obtained by methods assuming monotonic loading under drained condition, depending on the actual sand (e.g. grain size distribution and relative density) and storm load history. This paper considers calculation of the Ultimate Limit State (ULS) capacity of monopiles. It is acknowledged that the actual dimensions of the monopile may be governed by other design states and requirements. It is shown that the Partially Drained Cyclic Accumulation Model (PDCAM) may account for the effects of cyclic loading and dilatancy in the calculation of the capacity (here defined as a lateral cyclic displacement at seabed equal to 10% of the diameter). For an example calculation of a large diameter ($D = 9m$) monopile foundation into a homogeneous dense sand ($Dr = 80\%$) for a $10MW$ wind turbine at about 30 m water depth in the North Sea, a two-way peak storm loading condition (idling) needs an embedded depth of more than $15.8m$ ($L/D > 1.75$) to satisfy the displacement criterion. The corresponding required embedded depth found from a drained push-over analyses using the Hardening Soil Small strain (neglecting the effect of cyclic loading) is $12.5m$ ($L/D > 1.4$).

A simplified procedure PDCAM-S for evaluating the effect of cyclic loading under partially drained condition is also proposed. This procedure may be used together with almost all non-linear finite element programs. The main advantage of PDCAM-S is that the calculations are more robust and computationally more efficient than using PDCAM, albeit sacrificing some accuracy in the results. The input parameters to PDCAM-S should therefore be selected carefully to obtain results on the conservative side.

DATA AVAILABILITY STATEMENT

Some or all data, models, or code that support the findings of this study are available from the corresponding author upon reasonable request.

ACKNOWLEDGEMENT

The authors gratefully acknowledge the support from the Wave Loads and Soil Support for

Extra-Large Monopiles (WAS-XL) project (NFR grant 268182) and from the REDucing cost of offshore WINd by integrated structural and geotechnical design 2 (REDWIN 2) project (NFR grant 296511).

REFERENCES

Andersen, K. H. (2015). "Cyclic soil parameters for offshore foundation design." *Frontiers in offshore geotechnics III*, 5.

Andersen, K. H., Kleven, A., and Heien, D. (1988). "Cyclic soil data for design of gravity structures." *Journal of Geotechnical engineering*, 114(5), 517–539.

API (2014). *Recommended practice 2AWSD planning, designing and constructing fixed offshore platforms –working stress design, 22nd edn.* American Petroleum Institute.

Bachynski, E. E., Page, A., and Katsikogiannis, G. (2019). "Dynamic response of a large-diameter monopile considering 35-hour storm conditions." *International Conference on Offshore Mechanics and Arctic Engineering*, Vol. 58899, American Society of Mechanical Engineers, V010T09A064.

Blaker, Ø. and Andersen, K. H. (2019). "Cyclic properties of dense to very dense silica sand." *Soils and Foundations*, 59(4), 982–1000.

Brinkgreve, R., Kumarswamy, S., Swolfs, W., Waterman, D., Chesaru, A., Bonnier, P., et al. (2016). "Plaxis 2016." *PLAXIS bv, the Netherlands*.

Brinkgreve, R., Lisi, D., Lahoz, M., and Panagoulias, S. (2020). "Validation and application of a new software tool implementing the pisa design methodology." *Journal of Marine Science and Engineering*, 8(6), 457.

Byrne, B. W., Burd, H. J., Zdravkovic, L., Abadie, C. N., Houlsby, G. T., Jardine, R. J., Martin, C. M., McAdam, R. A., Pacheco Andrade, M., Pedro, A. M., et al. (2019). "Pisa design methods for offshore wind turbine monopiles." *Offshore Technology Conference*, Offshore Technology Conference.

DNV (2016). "DNVGL-ST-0126: Support structures for wind turbines." *Oslo, Norway: DNV GL.*

Erbrich, C., O'Neill, M., Clancy, P., and Randolph, M. (2010). "Axial and lateral pile design in carbonate soils." *Proc., 2nd International Symposium on Frontiers in Offshore Geotechnics (ISFOG II)*, 125–154.

Fan, S., Bienen, B., and Randolph, M. F. (2021). "Effects of monopile installation on subsequent lateral response in sand. i: Pile installation." *Journal of Geotechnical and Geoenvironmental Engineering*, 147(5), 04021021.

Femsys Limited (1999). "The finite element pre- and post-processor." *FEMGV 6.1*.

Grimstad, G., Andresen, L., and Jostad, H. P. (2012). "NGI-ADP: Anisotropic shear strength model for clay." *International journal for numerical and analytical methods in geomechanics*, 36(4), 483–497.

Jostad, H. P., Carotenuto, P., Yusuke, S., and Sivasithamparam, N. (2021). "Measuring and modelling cyclic response of dense sand under partially drained conditions." *International Conference of the International Association for Computer Methods and Advances in Geomechanics*, Springer, 447–455.

Jostad, H. P., Dahl, B. M., Page, A., Sivasithamparam, N., and Sturm, H. (2020). "Evaluation of soil models for improved design of offshore wind turbine foundations in dense sand." *Géotechnique*, 70(8), 682–699.

Jostad, H. P., Grimstad, G., Andersen, K., Saue, M., Shin, Y., and You, D. (2014). "A FE procedure for foundation design of offshore structures–applied to study a potential owt monopile foundation in the korean western sea." *Geotechnical Engineering Journal of the SEAGS & AGSSEA*, 45(4), 63–72.

Jostad, H. P., Grimstad, G., Andersen, K., and Sivasithamparam, N. (2015). "A FE procedure for calculation of cyclic behaviour of offshore foundations under partly drained conditions." *Frontiers in offshore geotechnics III*, 1, 153–172.

Li, S., Zhang, Y., and Jostad, H. P. (2019). "Drainage conditions around monopiles in sand." *Applied Ocean Research*, 86, 111–116.

Liu, H. Y., Diambra, A., Abell, J. A., and Pisanò, F. (2020). "Memory-enhanced plasticity modeling of sand behavior under undrained cyclic loading." *Journal of Geotechnical and Geoenvironmen-*

tal Engineering, 146(11), 04020122.

Liu, H. Y. and Kaynia, A. M. (2021). "Characteristics of cyclic undrained model sanisand-msu and their effects on response of monopiles for offshore wind structures." *Géotechnique*, 1–16.

Liu, H. Y., Kementzetzidis, E., Abell, J. A., and Pisanò, F. (2021). "From cyclic sand ratcheting to tilt accumulation of offshore monopiles: 3D FE modelling using sanisand-ms." *Géotechnique*, 1–16.

Liu, H. Y., Sivasithamparam, N., Suzuki, Y., and Jostad, H. P. (2022). "Load history idealization effects for design of monopiles in clay." *Géotechnique*, 1–30.

Matsuishi, M. and Endo, T. (1968). "Fatigue of metals subjected to varying stress." *Japan Society of Mechanical Engineers, Fukuoka, Japan*, 68(2), 37–40.

Niemunis, A. and Herle, I. (1997). "Hypoplastic model for cohesionless soils with elastic strain range." *Mechanics of Cohesive-frictional Materials: An International Journal on Experiments, Modelling and Computation of Materials and Structures*, 2(4), 279–299.

Potts, D. M., Zdravković, L., Addenbrooke, T. I., Higgins, K. G., and Kovačević, N. (2001). *Finite element analysis in geotechnical engineering: application*, Vol. 2. Thomas Telford London.

Schanz, T., Vermeer, P., and Bonnier, P. G. (1999). "The hardening soil model: formulation and verification." *Beyond 2000 in computational geotechnics*, Routledge, 281–296.

Staubach, P., Machaček, J., Sharif, R., and Wichtmann, T. (2021). "Back-analysis of model tests on piles in sand subjected to long-term lateral cyclic loading: Impact of the pile installation and application of the hca model." *Computers and Geotechnics*, 134, 104018.

Stewart, H. E. (1986). "Permanent strains from cyclic variable-amplitude loadings." *Journal of Geotechnical Engineering*, 112(6), 646–660.

List of Tables

TABLE 1. Load parcels of bending moment and horizontal force at seabed

Parcels	Cycles	Storm moment M (kNm)	Loading ratio	Time (s)
1	421	18575	0.05	1684
2	209	55727	0.15	2520
3	218	92879	0.25	3392
4	142	130030	0.35	3960
5	79	167181	0.45	4276
6	38	204333	0.55	4428
7	19	241484	0.65	4504
8	11	278636	0.75	4548
9	2	306500	0.825	4556
10	2	325075	0.875	4564
11	1	343651	0.925	4568
12	1	371515	1	4572

TABLE 2. Material parameters for HS-Small model

E_{50}^{ref} $[kN/m^2]$	E_{oed}^{ref} $[kN/m^2]$	E_{ur}^{ref} $[kN/m^2]$	m	ν_{ur}	K_0^{NC}	G_0^{ref}
60000	55000	160000	0.5	0.2	0.45	200000
$\gamma_{0.7}$ [%]	c'_{ref} $[kN/m^2]$	Φ' [°]	Ψ [°]	R_f	POP $[kN/m^2]$	
2	0	43.6	12	0.9	10000	

TABLE 3. Stress-strain curve fitting parameters

$(G_0/p'_0)^*$	$(\gamma_{psf})^*$ [%]	$(\tau_0/p'_0)^*$	$(\tau_{cy}/p'_0)_{max}$ N = 1	$ct(\tau_{cy}/p'_0)_{max}$ N = 3	$(\tau_{cy}/p'_0)_{max}$ N = 10	$(\tau_{cy}/p'_0)_{max}$ N = 30
500	21	0	4.4	3.6	2.2	1.5
*: The values are the same across N = 1, 3, 10, 30.						

TABLE 4. NGI-ADP model parameters

G_{ur}/s_u^A	γ_f^C [%]	γ_f^E [%]	γ_f^{DSS} [%]	$s_u^{C,TX}/s_u^A$	$s_{u_{ref}}^A$ [%]
$*/$	21	21	21	0.99	0.1
z_{ref} [m]	s_{uinc}^A $[kN/m^2/m]$	s_u^p/s_u^A	τ_0/s_u^A	s_u^{DSS}/s_u^A	ν_u
0	$*/$	1	0	1	0.49
$*/$: Depends on the τ_{cy}/p_0' values in Table 3					

TABLE 5. Equivalent number of cycles for each sublayer after iteration in PDCAM-S

Layer	1	2	3	4	5	6	7*
N_{eq} for initial estimation	6	6	6	6	6	6	6
N_{eq} after iteration 1	8	8	6	5	5	5	8
N_{eq} after iteration 2	8	8	7	5	5	5	8
*: The soil layer below pile tip							

TABLE 6. Soil reaction force ratio R_p with embedded length for all load parcels and global load ratio after each parcel. $L = 18m$ $(L/D = 2)$.

	Layer 1	**Layer 2**	**Layer 3**	**Layer 4**	**Layer 5**	**Layer 6**	**global load ratio**
Parcel 1	0.07	0.06	0.05	0.03	0.01	0.04	0.05
Parcel 2	0.21	0.18	0.15	0.12	0.08	0.11	0.15
Parcel 3	0.35	0.29	0.24	0.20	0.15	0.19	0.25
Parcel 4	0.48	0.40	0.34	0.28	0.23	0.26	0.35
Parcel 5	0.60	0.52	0.45	0.37	0.31	0.34	0.45
Parcel 6	0.70	0.64	0.55	0.46	0.39	0.42	0.55
Parcel 7	0.78	0.75	0.66	0.55	0.48	0.51	0.65
Parcel 8	0.84	0.84	0.77	0.65	0.58	0.63	0.75
Parcel 9	0.89	0.89	0.86	0.74	0.66	0.72	0.825
Parcel 10	0.92	0.92	0.91	0.80	0.73	0.80	0.875
Parcel 11	0.96	0.95	0.95	0.88	0.82	0.87	0.925
Parcel 12	1.00	1.00	1.00	1.00	1.00	1.00	1

List of Figures

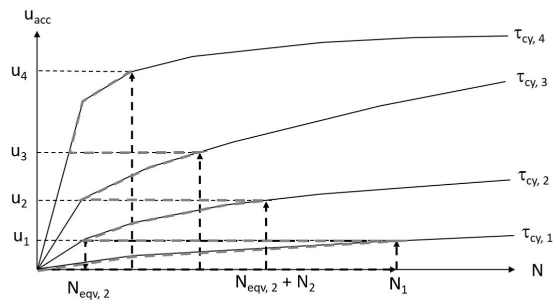

Fig. 1. Accumulated pore pressure u_{acc} versus number of loading cycles N and normalised cyclic shear stress τ_{cy}

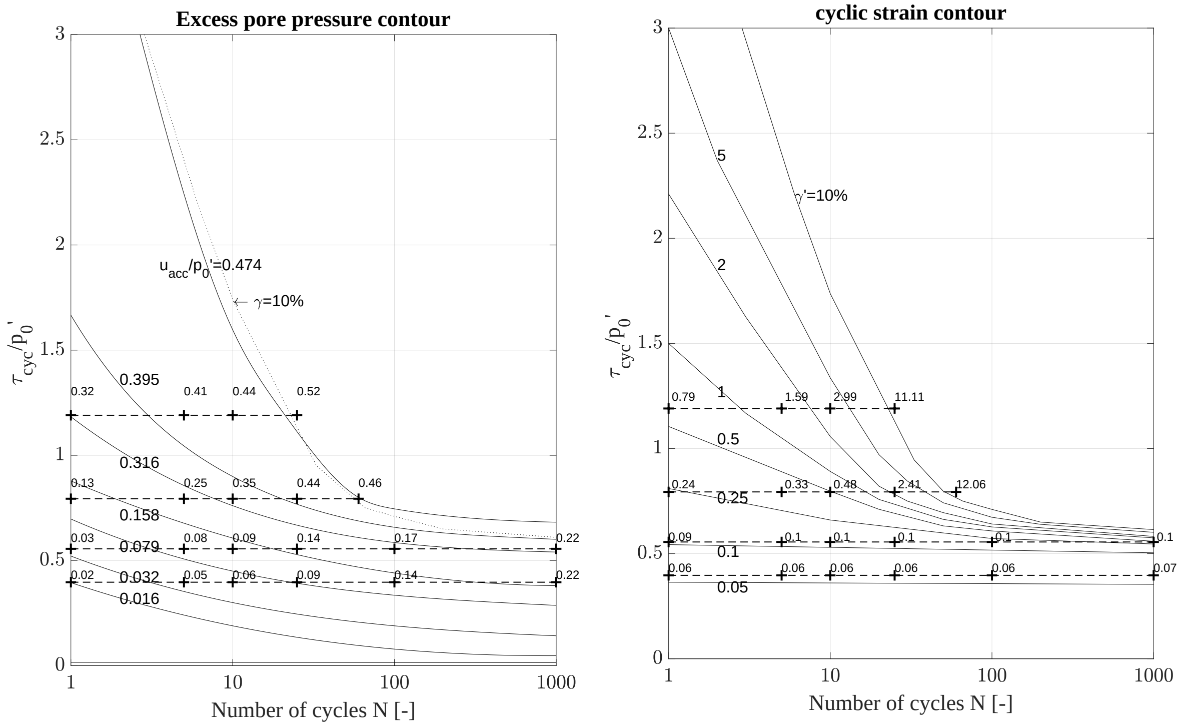

(a) Pore pressure contour diagram.

(b) Cyclic shear strain contour diagram.

Fig. 2. Examples of cross-sections of contour diagrams.

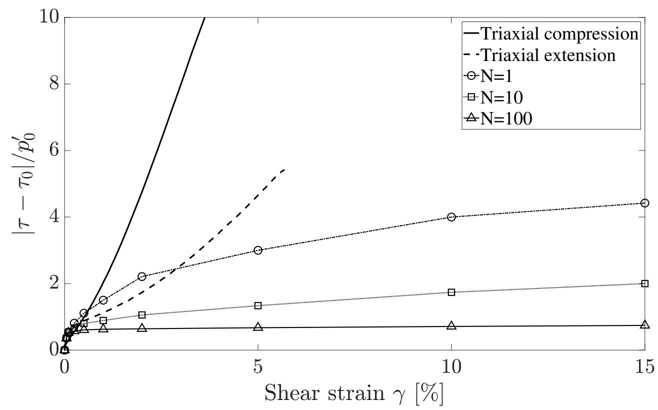

Fig. 3. Cyclic stress strain curves for $N = 1$, 10 and 100 extracted from cyclic strain contour diagram, compared with undrained monotonic triaxial compression and extension tests results. Test conditions: initial mean effective stress $p'_0 = 200$kPa, relatively density $D_r = 80\%$, $K_0 = 0.45$.

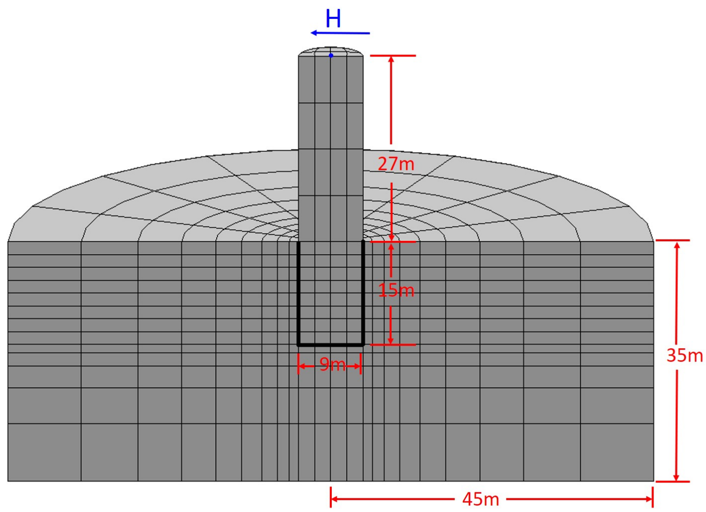

Fig. 4. Bifurc 3D FE model.

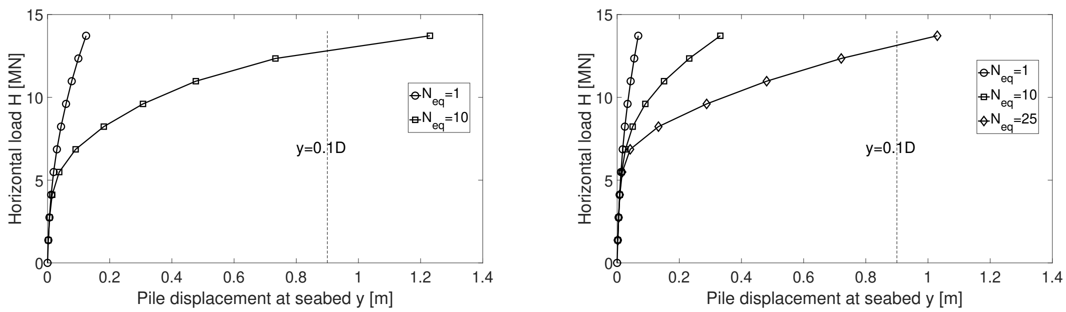

(a) Pile length $L = 15m$ $(L/D = 1.667)$ **(b)** Pile length $L = 18m$ $(L/D = 2)$

Fig. 5. Cyclic lateral displacement at seabed level. Cyclic horizontal load applied at $27m$ above seabed, $N_{eq} = 1$ and 10.

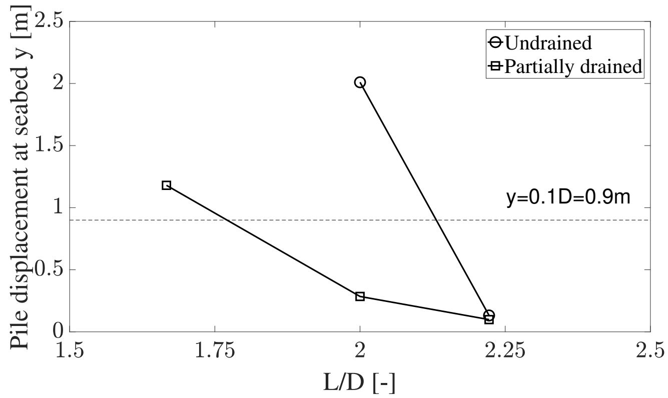

Fig. 6. Cyclic lateral displacement at the end of the storm history against different pile aspect ratios (L/D).

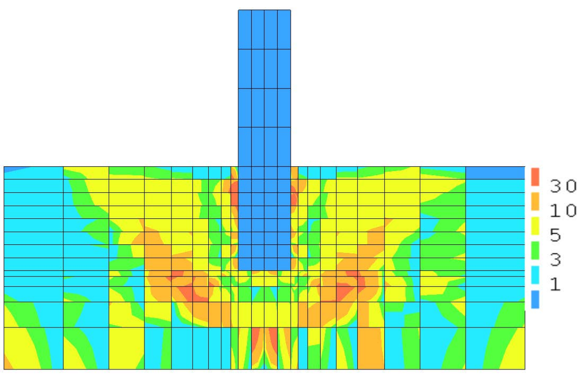

(a) Partially drained

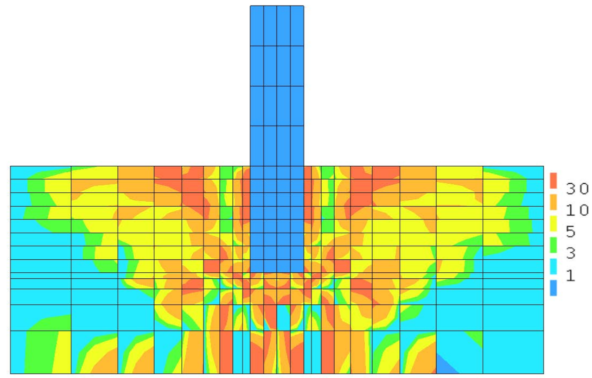

(b) Undrained

Fig. 7. Contours of equivalent number of cycles in a cross section cut along axis of symmetry (along loading direction), at the end of the storm. $L = 18m$ $(L/D = 2)$.

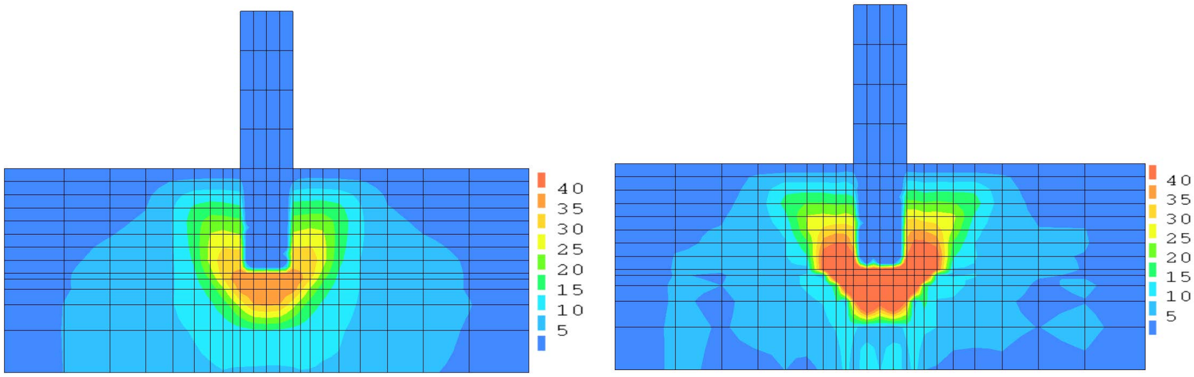

(a) Partially drained **(b)** Undrained

Fig. 8. Contours of accumulated pore water pressure (in the unit of kPa) in a cross section cut along axis of symmetry (along loading direction), at the end of the storm. $L = 18m$ ($L/D = 2$).

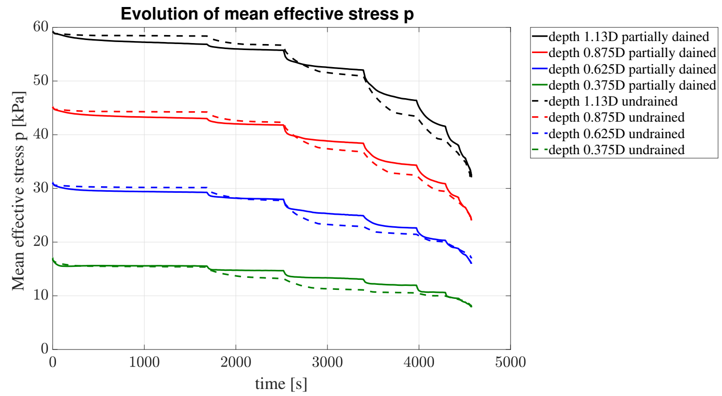

(a) Evolution of mean effective stress p'

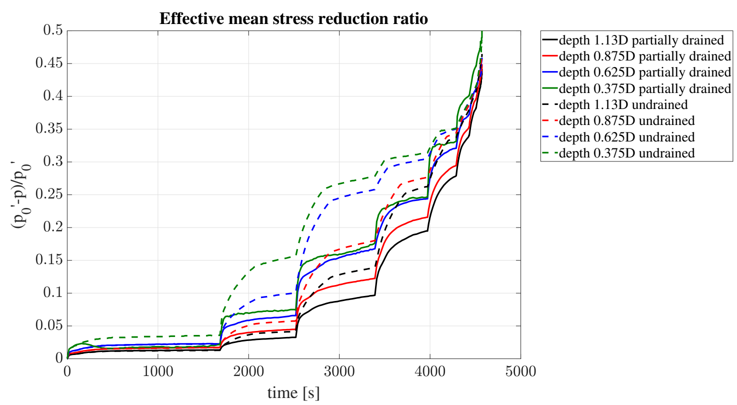

(b) Evolution of mean effective stress reduction ratio

Fig. 9. Mean effective stress change against time at four different depths, at the end of the storm. $L = 18m$ $(L/D = 2)$.

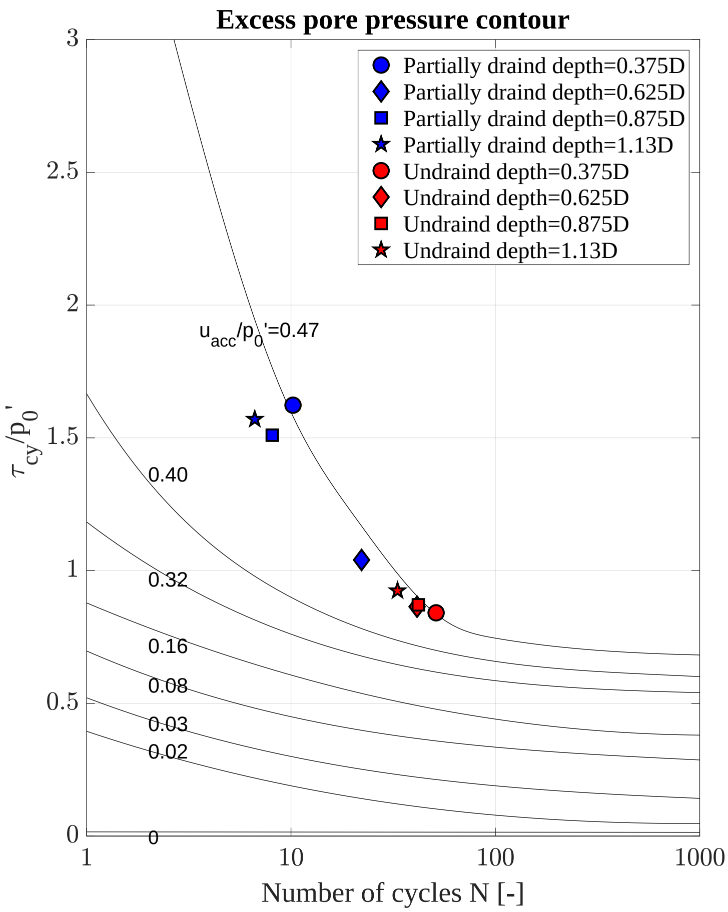

Fig. 10. End points in pore pressure contour diagram from pore pressure accumulation using PD-CAM. $L = 18m$ ($L/D = 2$).

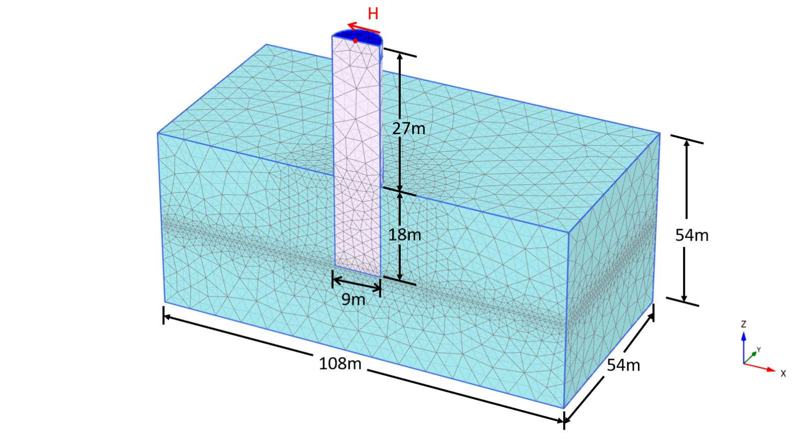

Fig. 11. Finite element model used in the PLAXIS model.

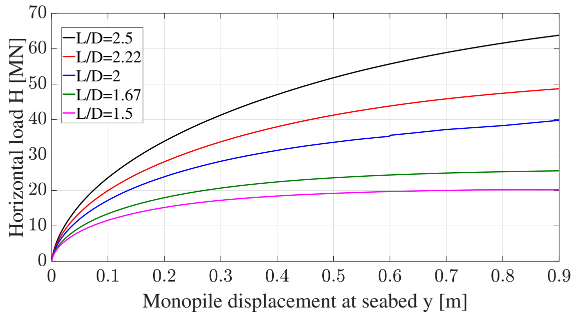

(a) Pile displacement against applied load

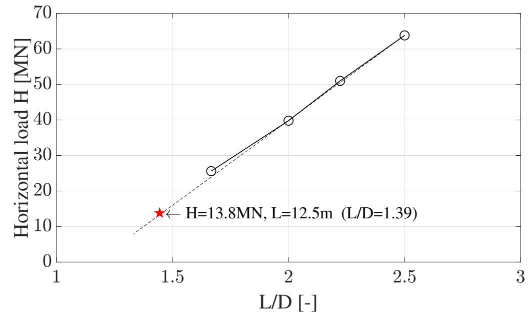

(b) Pile lateral capacity against pile L/D ratio

Fig. 12. Cyclic lateral displacement at the end of the storm history. Simulation conditions: fully drained domain, HS small model results. Pile lateral capacity defined as the load to cause $0.1D$ pile displacement at seabed level.

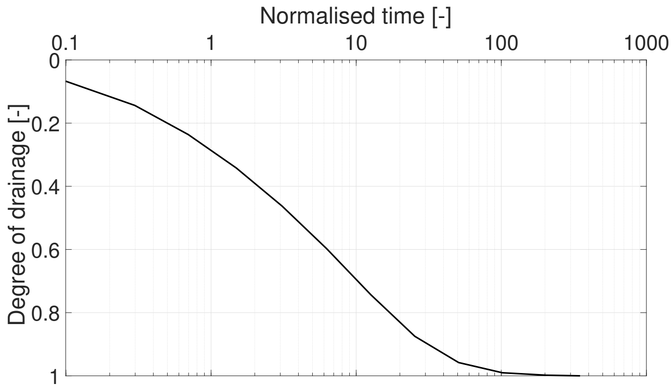

Fig. 13. Degree of drainage with normalised time.

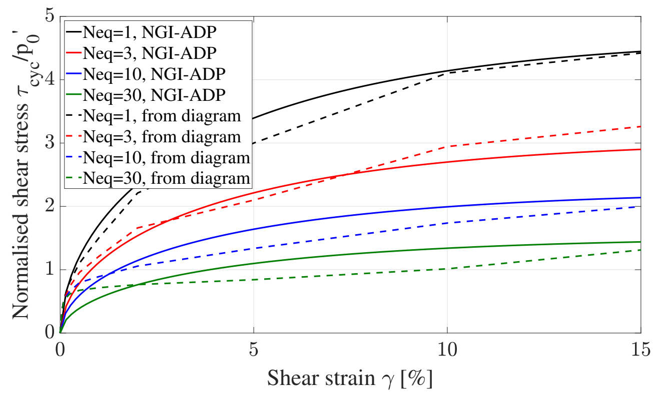

Fig. 14. Fitted cyclic shear stress-strain curves for N=1, 3, 10 and 30 using NGI-ADP.

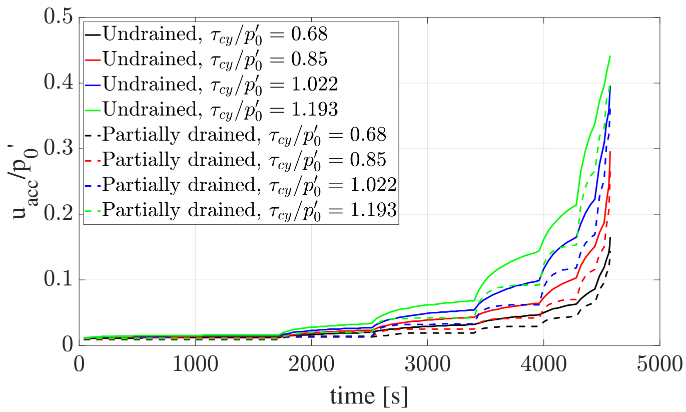

Fig. 15. Normalised pore pressure against time under different stress levels.

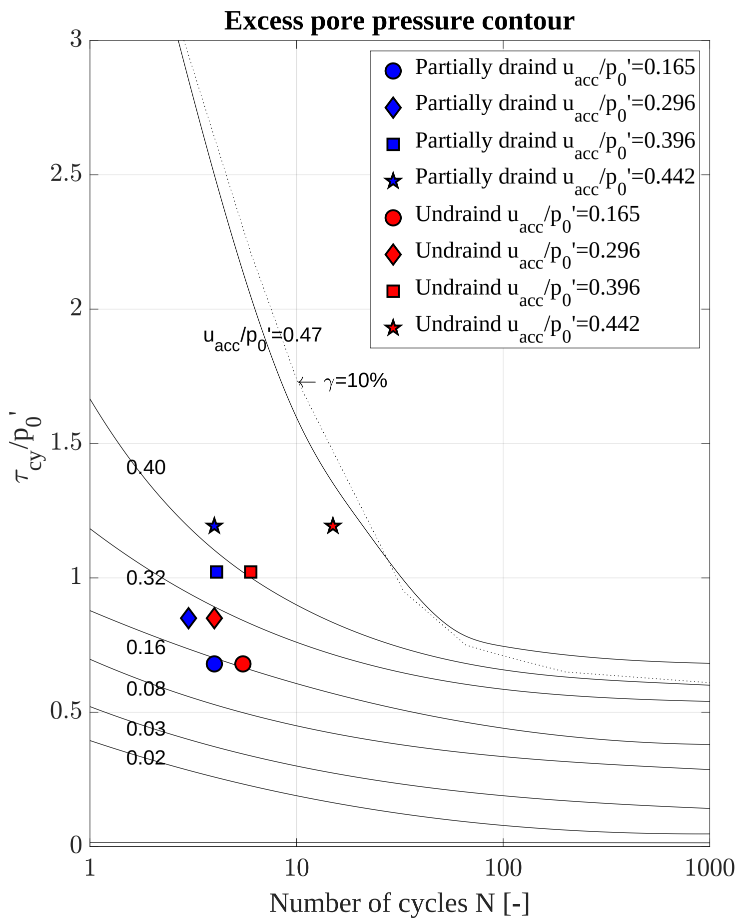

Fig. 16. Loci of end points in pore pressure contour diagram from pore pressure accumulation using PDCAM-S.

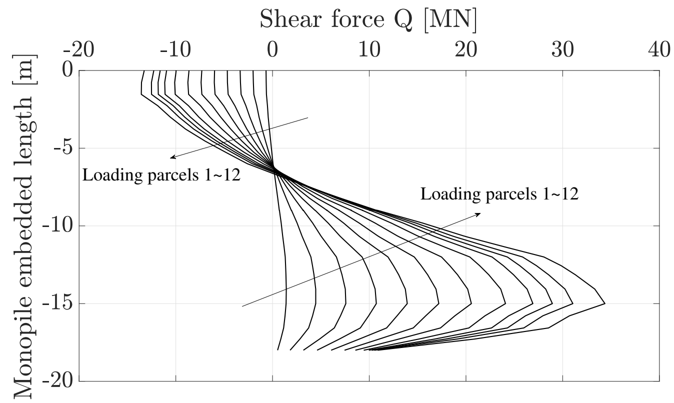

Fig. 17. Variation of shear force with embedded length for all load parcels. $L = 18m$ $(L/D = 2)$.